Research Article

Journal of PeptideScience

Received: 7 January 2009 Revised: 24 March 2009 Accepted: 24 March 2009 Published online in Wiley Interscience: 19 May 2009

(www.interscience.com) DOI 10.1002/psc.1144

Different mechanisms of action of antimicrobial peptides: insights from fluorescence spectroscopy experiments and molecular dynamics simulations‡

Gianfranco Bocchinfuso,[a] Antonio Palleschi,[a] Barbara Orioni,[a] Giacinto Grande,[a] Fernando Formaggio,[b] Claudio Toniolo,[b] Yoonkyung Park,[c] Kyung-Soo Hahm[c] and Lorenzo Stella[a]*

Most antimicrobial peptides exert their activity by interacting with bacterial membranes, thus perturbing their permeability. They are investigated as a possible solution to the insurgence of bacteria resistant to the presently available antibiotic drugs. However, several different models have been proposed for their mechanism of membrane perturbation, and the molecular details of this process are still debated. Here, we compare fluorescence spectroscopy experiments and molecular dynamics (MD) simulations regarding the association with lipid bilayers and lipid perturbation for two different amphiphilic helical antimicrobial peptides, PMAP-23 and trichogin GA IV. PMAP-23, a cationic peptide member of the cathelicidin family, is considered to induce membrane permeability according to the Shai-Matsuzaki-Huang ''carpet'' model, while trichogin GA IV is a neutral peptide, member of the peptaibol family. Although several lines of evidence suggest a ''barrel-stave'' mechanism of pore formation for the latter peptide, its length is only half the normal thickness of a lipid bilayer. Both fluorescence spectroscopy experiments and MD simulations indicated that PMAP-23 associates with membranes close to their surface and parallel to it, and in this arrangement it causes a severe perturbation to the bilayer, both regarding its surface tension and lipid order. By contrast, trichogin GA IV can undergo a transition from a surface-bound state to a transmembrane orientation. In the first arrangement, it does not cause any strong membrane perturbation, while in the second orientation it might be able to span the bilayer from one side to the other, despite its relatively short length, by causing a significant thinning of the membrane.

Keywords: antimicrobial peptides; fluorescence spectroscopy; molecular dynamics simulations; peptide-membrane interactions

Introduction

Antimicrobial peptides (AMPs) constitute an important part of the innate defense of all organisms, including man [1]. Their main activity is bactericidal, and it is mediated by their interaction with the cellular membrane of pathogens and perturbation of its permeability, leading to cell death due to osmotic shock and leakage of intracellular material [2]. Development of bacterial resistance to AMPs is much less likely than for traditional antibiotics, as a consequence of their target and their mechanism of action [3]. For this reason, these peptides are investigated as lead compounds for the development of a new class of antibiotic drugs [4]. However, even after many years of research on AMPs, a detailed understanding of the molecular details of their mechanism of membrane perturbation, which would allow the design of new molecules with improved activity, selectivity and bioavailability, is still elusive.

AMPs are very diverse regarding their length, sequence and secondary structure [5], but the most common and extensively investigated class is formed by amphipathic helical peptides [6]. The molecules belonging to this class are long up to 40 residues and attain a helical conformation after association with the lipid membranes. In this structure, the side chains are arranged amphiphilically, with apolar and hydrophilic residues segregated in two different faces of the helix.

Several models have been proposed to account for the permeabilization of lipid membranes by these AMPs. One of the first hypotheses put forward was the ''barrel-stave'' mechanism [7], according to which peptides insert into the membrane in a transbilayer orientation, and aggregate to form a pore, with their hydrophilic faces lining the water-filled lumen of the channel and their apolar residues pointing towards the membrane. Even though this model was proposed more than 30 years ago, a

* *Correspondence to: Lorenzo Stella, Dipartimento di Scienze e Tecnologie Chimiche, Università di Roma Tor Vergata, via della Ricerca Scientifica 1, 00133 Roma, Italy. E-mail: stella@stc.uniroma2*

a *Department of Chemical Sciences and Technologies, University of Rome ''Tor Vergata'', 00133 Rome, Italy*

b *Institute of Biomolecular Chemistry, Padova Unit, CNR, Department of Chemistry, University of Padova, 35131 Padova, Italy*

c *Research Center for Proteineous Materials, and Department of Cellular and Molecular Medicine, School of Medicine, Chosun University, 501-759 Gwangju, Korea*

‡ *Special issue devoted to contributions presented at the 1st Italy-Korea Symposium on Antimicrobial Peptides, 24–25 July 2008.*

Journal of PeptideScience

conclusive demonstration of its validity was obtained only for the peptaibol alamethicin [8–10].

Another mechanism, called the ''carpet'' model, was proposed more recently by Shai, Matsuzaki and Huang [11–13], and it involves the association of AMPs with the membrane surface, parallel to it, with the hydrophilic face of the helix oriented towards the water phase. According to this model, membrane perturbation is caused by the strain produced in the outer layer of the membrane by peptide insertion. When a threshold membrane-bound peptide/lipid ratio is reached, this strain is released by the formation of membrane defects. Within this general scheme, different versions of the model have been proposed: for instance Huang and co-workers [13] reported experimental data indicating that the membrane permeability is due to pores with a well-defined toroidal structure, in which the membrane bends back onto itself in a doughnut shape, and the peptides are interspersed between the phopholipid heads lining the curved pore surface. More recently, MD simulations suggested that the pore structure might be much less well defined, leading to the proposal of the so-called ''disordered toroidal pore model'' [14,15].

In addition to these two main models, several other hypotheses have been put forward, such as the ''sinking raft'' model [16], in which several peptides form an aggregate, which can diffuse through the membrane, or the ''leaky slit'' model [17], in which the peptides are oriented perpendicularly to the membrane, but, rather than forming a circular pore, they aggregate side to side to form an amphipathic ribbon. The hydrophobic face of the ribbon is oriented towards the hydrocarbon chains of the bilayer, while toxicity is caused by the hydrophilic face, as this side of the ribbon cannot seal with the opposing contacting bilayer by hydrophobic interactions. As a consequence, lipids are forced to adopt a highly positive curvature, causing the membrane to bend onto itself.

As evidenced by the variety of models put forward, the situation is rather complex and different mechanisms have been proposed to apply for the same peptide, depending on the specific techniques and experimental conditions used to investigate them [18,19]. For this reason, Bechinger and Lohner [20] suggested that different mechanism could actually apply under different conditions to the same peptide, with the only common principle that AMPs' activity is somewhat similar to the membrane-disrupting properties of detergents.

This lack of clarity on the mechanism of action of AMPs is due mainly to the difficulty in obtaining atomic-resolution structural data on peptide-membrane systems [21]. For this reason, we have recently proposed to use synergistically MD simulations and fluorescence spectroscopy experiments to study the interaction of membrane-active peptides with lipid bilayers [22]. Fluorescence experiments can provide low-resolution data on the position and orientation of AMPs inside a membrane, and on their effect on the bilayer structure [23], while MD simulations yield an unparalleled detail on peptide structure, dynamics and membrane-perturbing effects in a bilayer [14,15,24–26]. If the MD simulations are validated by comparison with the fluorescence data, their atomic details can be used to obtain new insights into the mechanism of membrane perturbation by AMPs.

This approach has recently been applied to the cationic, 23-mer AMP PMAP-23 [22]. Here, we report similar simulations on the 10-mer peptide trichogin GA IV, which had already been extensively studied by fluorescence spectroscopy experiments [27–32], and we discuss the differences in the behavior of these two peptides, representative of two large classes of helical AMPs.

Table 1. Amino acid sequences of the peptides investigated

PMAP-23	RIIDLLWRVRRPQKPKFVTVWVR
Trichogin GA IV[a]	*n*-Oct-UGLUGGLUGILol

[a] *n*-Oct = *n*-octanoyl; U = Aib, α-aminoisobutyric acid; Lol = leucinol.

The amino acid sequences of PMAP-23 and of trichogin GA IV, reported in Table 1, evidence the different characteristics of these peptides. PMAP-23 [33–37] contains seven basic residues and is therefore a typical representative of the class of cationic AMPs [38]. A high content of cationic residues is one of the most common traits of helical AMPs, and it is thought to be an important property for a selective membranolytic activity, because bacterial membranes contain a much higher proportion of negatively charged lipids than those of eukaryotes. Trichogin GA IV [27–32,39,40] belongs to the class of peptaibols [41–43], another extensively investigated group of AMPs, the most well-known member of which is alamethicin [8–10,44]. These peptides, synthesized non-ribosomially by fungi, contain unusual aminoacids (such as Aib, α-aminoisobutyric acid), a C-terminal 1,2-aminoalcohol and an N-terminal acyl chain. They are distinctly hydrophobic, comprising only a few polar or charged residues.

Different mechanisms of action can be envisaged for PMAP-23 and for trichogin GA-IV. Because of their charge, it is highly unlikely that cationic peptides could insert into lipid membranes, so that a consensus has been reached that they usually act according to the ''carpet'' model. We have recently reported experimental evidence supporting this conclusion in the specific case of PMAP-23 [22]. By contrast the peptaibol alamethicin is the most clear-cut example of a peptide acting according to the ''barrel-stave'' mechanism. Our fluorescence spectroscopy experiments [28] support the same mechanism of membrane perturbation for trichogin GA IV. However, the length of this peptide in its helical conformation is only about half the normal thickness of a lipid bilayer, so that the structure of the trichogin pores remained to be defined.

For these reasons, we chose to concentrate this study on a comparison between trichogin GA IV and PMAP-23, by combining MD simulations and fluorescence experiments on the location and effects of these two peptides inside lipid membranes, so as to identify the hallmarks of each mechanism of action.

Materials and Methods

Materials

Phospholipids were purchased from Avanti Polar Lipids (Alabaster, AL). The total chemical synthesis in solution of trichogin GA IV and its equipotent trichogin analogue Tric-OMe, where the N-terminal leucinol was replaced by a leucine methyl ester [40], was performed according to Toniolo *et al.* [45], while the synthesis of PMAP-23 was already described [22]. Peptide purity (>98%) was confirmed by HPLC and mass spectrometry (data not shown).

Peptide Effects on Lipid Phase Transition

Large unilamellar vesicles were prepared as previously described [27]. Liposomes were formed by DMPC (1,2-dimyristoyl-*sn*-glycero-3-phosphocholine) or DMPC/DMPG (1,2-dimyristoyl-*sn*-glycero-3-[phospho-*rac*-(1-glycerol)]) in a 2:1 molar ratio, and contained the fluorescent probe (DPH) 1,6-diphenylhexatriene in

a fluorophore/lipid molar ratio of 1 : 100. Lipids were hydrated in a 10 mM phosphate buffer (pH 7.4), containing 140 mM NaCl, and 0.1 mM EDTA. The total lipid concentration is always reported. Steady-state fluorescence anisotropy measurements were carried out on a Fluoromax 2 fluorimeter (SPEX, Edison, NJ) equipped with automated Glan-Thompson polarizers, with excitation and emission wavelengths of 350 nm and 450 nm, respectively, 4 nm band pass, a WG385 cut-off filter in the emission channel, and averaging nine replicate determinations for each measurement. Temperature was controlled by a thermostatted cuvette holder to within 0.1 °C. In the case of PMAP-23, 50 mM DMPC/DMPG vesicles were used and a 10 μM peptide concentration, while for Tric-OMe 200 mM DMPC vesicles were used and a 24 μM peptide concentration.

MD Simulations

MD simulations were performed according to the "minimum bias" method previously described [26]. Trichogin GA IV was initially shaped in its X-ray determined structure [46], and positioned at the centre of a cubic box with a side of 8.5 nm. A total of 128 POPC (1-palmitoyl-2-oleoyl-*sn*-glycero-3-phosphocholine) molecules, with different conformations taken from equilibrated simulations of phospholipid bilayers [47], and 5000 water molecules were added randomly in the box. MD simulations were performed with GROMACS 3.3, using ffgmx parameters [48]. The simple point charge (SPC) model was used for water [49], and water geometry was constrained with the SETTLE algorithm [50]. POPC parameters were previously reported [51,52]. A Berendsen thermostat, with a coupling constant of 0.1 ps, was applied in all simulations [53]. The reference temperature was set to 300 K, except where stated otherwise. Pressure coupling was applied anisotropically, also using the Berendsen scheme, with a time constant of 1.0 ps and a reference pressure of 1 bar. Bond lengths were constrained with the LINCS algorithm [54]. Short-range electrostatics and Lennard-Jones interactions were cut-off at 1.0 nm and long range electrostatic interactions were calculated using the particle mesh Ewald algorithm [55,56]. Simulations were run with a 4 fs timestep, removing fast hydrogen vibrations according to Feenstra *et al*. [57]. The system was energy-minimized and a first 100 ps equilibration MD run was performed with position restraining on the peptide. Molecular graphics were obtained with the program VMD [58]. Order parameters for the C-C bonds of the palmitic chains, were calculated with respect to the bilayer normal according to the following equation [59]:

$$S = \frac{3\langle \cos^2(\theta) \rangle - 1}{2}$$

where θ is the angle between the bilayer normal and the bond under consideration.

Results and Discussion

Peptide Location Inside the Lipid Bilayer

To characterize trichogin GA IV location inside lipid membranes via MD simulations, we used the recently proposed minimum bias approach [26], which was already successfully applied to PMAP-23 [22]. At present, an all-atoms MD simulation of a relatively large system, such as a hydrated phospholipid bilayer, can attain trajectory lengths in the 0.1–1 μs range. In many cases, this time-scale is insufficient to follow the association of a peptide to a preformed lipid bilayer and its reorientation inside the membrane towards the position and orientation corresponding to the global free-energy minimum. A possible alternative approach is to start from a completely random distribution of phospholipids, water and peptide into the simulation space, and to follow the spontaneous self-assembly of the membrane. The high initial mobility of such a disordered system ensures that the peptide is able to locate at the most favorable position in the water–membrane system.

To test the reliability of the results, three independent simulations were performed with different initial random configurations of water and lipids, and with trichogin GA IV initially shaped in the helical conformation determined by X-ray diffraction [46]. In agreement with previous applications of this approach [22,26,60–62], a rapid separation of the water and lipid phases was observed in all simulations (in less than 25 ns), followed by a reordering of the phospholipids towards a bilayer arrangement, in which, however, a rather stable water-filled pore was still present (Figure 1). This membrane defect healed spontaneously in one of the three simulations, while in the two other trajectories it was still present after 100 ns of simulation. In these cases, it was eliminated with a gentle annealing protocol, in which the system was cycled twice between 300 K and 375 K (rising the temperature linearly in 2 ns, decreasing it in 50 ps, and keeping it constant at 300 K for 950 ps). This annealing protocol did not cause significant modifications in the peptide conformation or in its position. After the water channel was eliminated, the trajectories were extended for further 10 ns, keeping the temperature at 300 K. All data analyses were performed on these final equilibrated trajectory segments.

In all cases, the helical conformation of trichogin GA IV was essentially maintained during the whole trajectory length, confirming the high helical propensity bestowed on this peptide by the Aib residues. In addition, in all simulations, trichogin GA IV positioned at the water–lipid interface, essentially parallel to it, since the very early stages of the trajectories. In two of the three simulations, this arrangement resulted in a final peptide orientation parallel to the membrane plane, a position just below the polar headgroups region, and a helix rotation such that all hydrophobic side chains were pointing towards the lipid bulk of the bilayer (Figure 2, top panel). However, in the third simulation, trichogin GA IV reached a final orientation parallel to the bilayer normal (Figure 3, left panel). It is interesting to note how this final configuration was attained (Figure 1, bottom panels): in the first stages of the trajectory the peptide located at the boundary between the water and lipid phases, as in all other cases. However, by contrast to the other two simulations, in this trajectory the bilayer formed perpendicularly to the trichogin GA IV molecule. The peptide was still located at the water–membrane interface, lining the water-filled membrane defect which was transiently present in all simulations. When this bilayer defect healed spontaneously, the peptide remained in a transmembrane orientation, fully immersed in the membrane hydrophobic core, and this configuration was stably maintained for all the remaining length of the trajectory (Figure 3, right panel).

The position determined by these MD simulations for trichogin GA IV differs from the location previously observed for the cationic peptide PMAP-23 [22] (Figure 2, bottom panel), under two respects: the latter peptide was always found to lie parallel to the membrane plane, and at a shallower depth than trichogin GA IV. The average position of the trichogin GA IV backbone atoms

Journal of PeptideScience

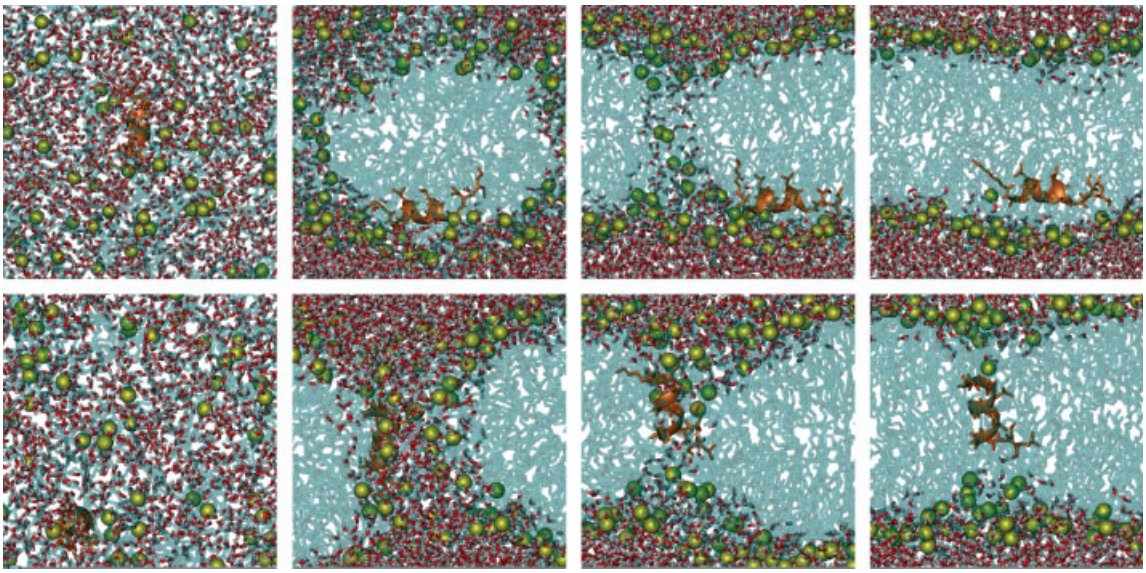

Figure 1. Bilayer formation during two different MD simulations of a trichogin GA IV–POPC system (top and bottom panels). The panels represent, from left to right, the situation at the beginning of the simulation, after 30 ns, after 100 ns (top series) or 70 ns (bottom series) and at the end of the trajectory. Water oxygen atoms are colored in red and hydrogen atoms in white. Phospholipid phosphorus atoms are represented as yellow spheres and the acyl chains are colored in cyan. The peptide is shown in orange.

was found to be at 0.8 nm below the phosphorus atoms of the phospholipids, while that of PMAP-23 was at a depth of just 0.4 nm, as illustrated also in Figure 2.

The two locations observed for trichogin GA IV are in perfect agreement with all available experimental data. We have shown through depth-dependent fluorescence quenching experiments [28–30] that trichogin GA IV undergoes a two-state transition from an inactive form, which is monomeric and lies close to the membrane surface, parallel to it, to an aggregated state, responsible for membrane leakage, where the peptide is more deeply buried into the phospholipid bilayer. This transition is controlled by peptide concentration, with the monomeric, surface bound form prevailing at membrane-bound peptide to lipid molar ratios below 0.01. These conclusions were more recently confirmed independently through electron paramagnetic resonance (EPR) experiments [63]. In our simulations, the peptide-to-lipid ratio was 1: 128, and indeed the calculations showed a preferred superficial location of the peptide. This position can be compared quantitatively with the results of the depth-dependent quenching experiments, which determined the position of fluorophores covalently linked to the N-terminus of the main chain or to selected side chains of trichogin GA IV. In these experiments (previously reported in [28,29]), a fluorescently labeled peptide interacts with vesicles containing lipids labeled with a doxyl moiety at a specific position along their acyl chain. Because doxyls cause fluorescence quenching through short-range interactions, a maximal quenching efficiency is observed when the depth of the quenching moiety and of the fluorophore inside the membrane coincide. As shown in Figure 4, both theoretical and experimental data indicate a fluorophore position at approximately 1 nm from the bilayer centre for the two trichogin GA IV analogues. The larger width of the experimental quenching profile, as compared to the density distribution obtained from simulations, is justified by the fact that the former results from the convolution of the distribution of depths populated by both fluorophore and lipid-attached quencher. A similar agreement was recently found also in the case of PMAP-23 [22], but it must be mentioned that in that case the curve determined by depth-dependent quenching experiments was much less well defined than in the

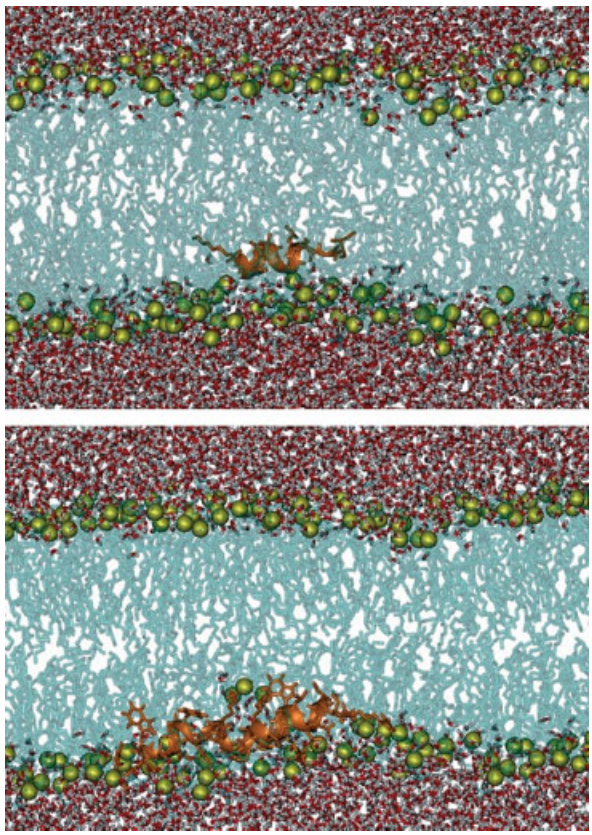

Figure 2. Top panel: Representative structure displaying the trichogin GA IV location in the surface-bound state at the end of one of the simulations. Bottom panel: Representative structure displaying the PMAP-23 location at the end of one of the simulations of [22]. The color coding is the same as in Figure 1.

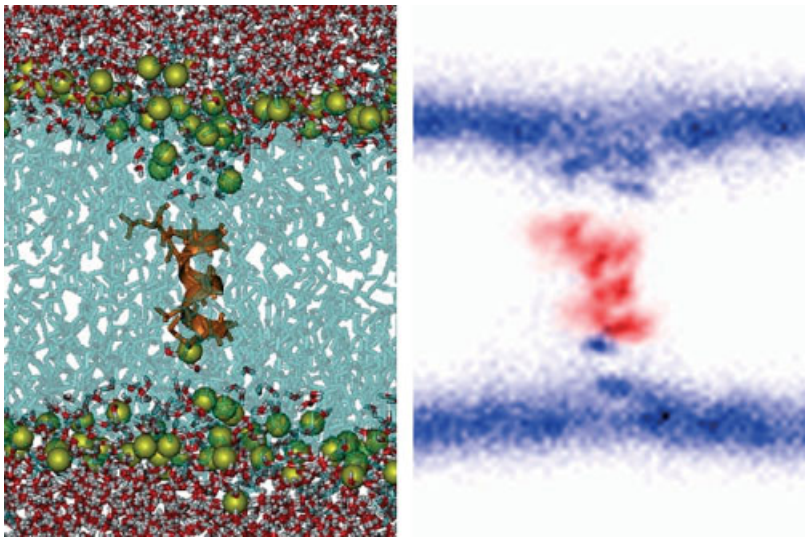

Figure 3. Left panel: Representative structure displaying trichogin GA IV location in the membrane inserted state at the end of one of the simulations. Right panel: Density map of the lipid phosphorus atoms (blue) and of the peptide atoms (red) averaged over the last 10 ns of the trajectory in which trichogin GA IV attained a transmembrane orientation.

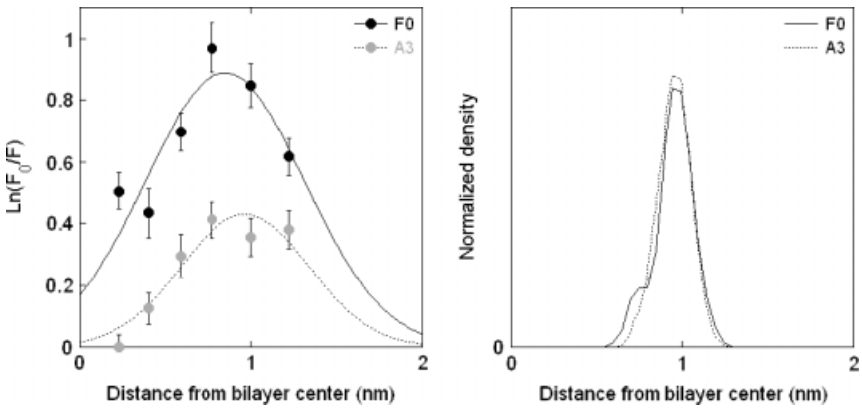

Figure 4. Comparison between the position of trichogin GA IV determined experimentally and from MD simulations. Left panel: Depth-dependent quenching experiments for the determination of the immersion depth of two fluorophores covalently linked to trichogin GA IV analogues at different positions (originally reported in [28,29]). In the analogue F0, a fluorenyl-9-methyloxycarbonyl moiety replaced the N-terminal *n*-octanoyl group of trichogin GA IV [29], while in the analogue A3 a β-(1-azulenyl)-alanine residue replaced Leu at position 3 [28]. The ordinate values are the natural logarithms of the ratio between the fluorescence intensities measured when the peptide was associated to unlabeled vesicles (F_0) and when it was bound to vesicles containing lipids labeled with a doxyl quencher at a specific position (F), indicated by the abscissa values. The details of the experiments are reported in [28–30]. The lines represent a Gaussian fit to the experimental data. Right panel: Normalized density profile of the position of the trichogin GA IV atoms corresponding to the fluorescent labels studied experimentally, averaged over the last 10 ns of one of the two trajectories with the peptide in a surface-bound state. The position of the fluorenyl fluorophore of the F0 analogue was approximated by the C_δ atom of the *n*-octanoyl chain of trichogin GA IV, while for the azulenyl group of the analogue A3, the $C_{\delta1}$ and $C_{\delta2}$ atoms of the side chain of the Leu residue at position 3 were used.

case of trichogin. This was attributed to the disorder caused by PMAP-23 in the organization of the phospholipid bilayer, as will be further discussed below. In addition, at all concentrations investigated, neither depth-dependent quenching experiments nor MD simulations ever indicated the presence of a membrane-inserted PMAP-23 configuration.

A further difference between trichogin GA IV and PMAP-23 was experimentally observed regarding the ability of the two peptides to translocate across the membrane. Förster resonance energy transfer experiments have shown that trichogin GA IV is able to translocate across the bilayer, distributing in both leaflets of the membrane, even at concentrations below its activity threshold, where it is not causing membrane leakage [28]. By contrast, in this concentration range PMAP-23 remains associated with the outer layer of the vesicles [22]. This result is a further indication that, even at concentrations below the activity threshold, an inserted location is possible for trichogin GA IV, at least transiently, as observed in one of our simulations, while the same location is not possible for the cationic peptide PMAP-23.

Peptide Effects on Lipid Order

Another interesting comparison regards the effects of the two peptides on the membrane to which they are associated. The approach used in our simulations allows a straightforward determination of the effects of peptide binding on the surface tension of the membrane, because in our method the lipids are able to distribute relatively rapidly between the two leaflets of the membrane even after the peptide is already located at its final position, as toroidal membrane defects are present until the final

Journal of PeptideScience

stages of the simulation. Table 2 shows the number of lipids which was present, after healing of all membrane defects, in the leaflet containing the peptide and in the opposite leaflet in all simulations performed for PMAP-23 (described in [22]) and trichogin GA IV (this article). Although PMAP-23 perturbs significantly the membrane, with a difference in the number of lipids in the two leaflets of 8–10 molecules, no significant perturbation was observed in the case of trichogin GA IV. This result could be due, in part, to the smaller dimensions of the trichogin GA IV peptide, but this difference cannot account for the whole effect, and the immersion depth of the two peptides probably plays a role.

Other differences in the effects caused by membrane association of the two peptides can be highlighted by calculating the order parameter for the lipid acyl chains with respect to the bilayer normal in the simulated trajectories [59]. This parameter, defined in the Materials and Methods Section, provides a quantitative estimate of the extent of lipid chain orientation along the bilayer normal, i.e. of the structural order of the membrane. A considerable difference in the lipid order was observed between the peptide-containing and the peptide-free bilayer leaflets in the case of PMAP-23, while these differences were not significant in the two simulations with a surface-bound trichogin GA IV (Figure 5). This conclusion was confirmed by fluorescence experiments on the effects of PMAP-23 and the equipotent synthetic trichogin GA IV analogue Tric-OMe [41] on the gel to liquid-crystal thermotropic phase transition of dimyristoyl phospholipids. The phase transition was followed by measuring the steady-state anisotropy of a membrane-inserted fluorophore (DPH), which reflects the probe mobility in the lipid bilayer, and therefore the fluidity of the membrane [64]. Tric-OMe had no effect on the thermotropic behavior, while PMAP-23 caused a significant perturbation of the phase transition (Figure 6). The peptide effects on lipid order observed for PMAP-23 are probably the cause for the ill-defined depth-dependent quenching profiles determined for this peptide [22].

Finally, it is interesting to discuss the effects of trichogin GA IV on the bilayer structure when it is arranged in a transmembrane orientation. Notwithstanding the relatively short length of the peptide helix, which is only about half the normal thickness of the bilayer, trichogin GA IV is able to span the bilayer from one side to the other by causing a local thinning of the membrane, as evidenced by the density map averaged over the last 10 ns of the trajectory reported in Figure 3 (right panel), accompanied by a deeper penetration of water molecules in the bilayer. This effect might be related to the well-known phenomenon called "hydrophobic mismatch" [65–67]: when hydrophobic molecules inserted into lipid membranes do not match the normal thickness of the bilayer, then the membrane adapts itself by thickening or thinning to match its size to that of the inserted molecule, thus minimizing the exposure of hydrophobic moieties to the water phase.

The present results might provide a solution to the long-standing puzzle regarding the mechanism of action of trichogin GA IV. Notwithstanding the experimental evidence supporting a barrel-stave mechanism of action for this peptide, it was thought that the short length of its chain would require a complex (and unlikely) supramolecular architecture to form the pore, e.g. with two peptide chains stacked on top of each other to span the bilayer from one side to the other. However, our simulations indicate that this is not necessary and that, thanks to the plasticity of the bilayer membranes, even a single trichogin GA IV chain might able to reach both sides of the bilayer.

Table 2. Phospholipid distribution in the two leaflets of the membrane in different simulations[a]

Peptide	Bilayer leaflet	1st MD	2nd MD
PMAP-23	Peptide-containing	60	59
	Peptide-free	68	69
Trichogin GA IV	Peptide-containing	63	65
	Peptide-free	65	63

[a] PMAP-23: MD simulations reported in [22]; trichogin GA IV: this article.

Conclusions

Combined MD simulations and fluorescence data showed that the two AMPs PMAP-23 and trichogin GA IV exhibit very different behaviours both regarding their position inside the lipid-bilayer and their effects on the membrane structure. The cationic PMAP-23 associates with membranes at a very shallow

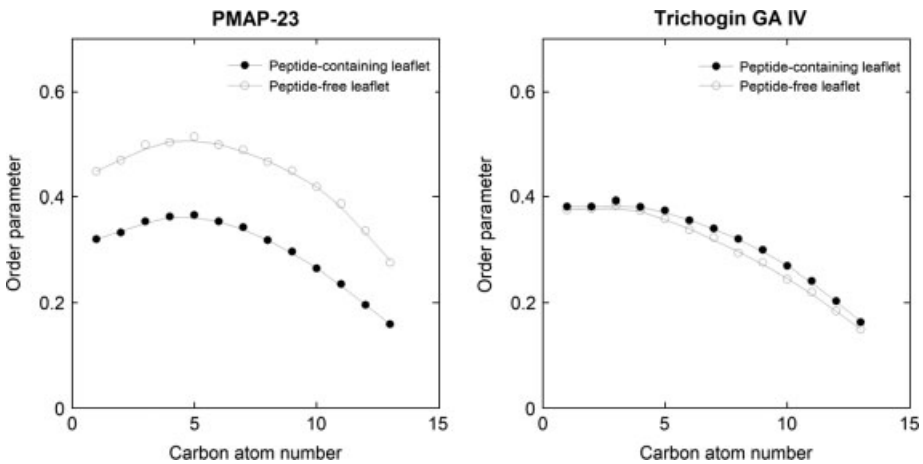

Figure 5. Order parameters with respect to the bilayer normal for the C_i–C_{i+1} bonds of the palmitic lipid chains, for the peptide-containing (full circles) and peptide-free (empty circles) leaflets of the membrane in the two simulations of PMAP-23 reported in [22] (left panel) and in the two simulations with the surface bound trichogin GA IV (right panel), averaged over the last 10 ns of both trajectories.

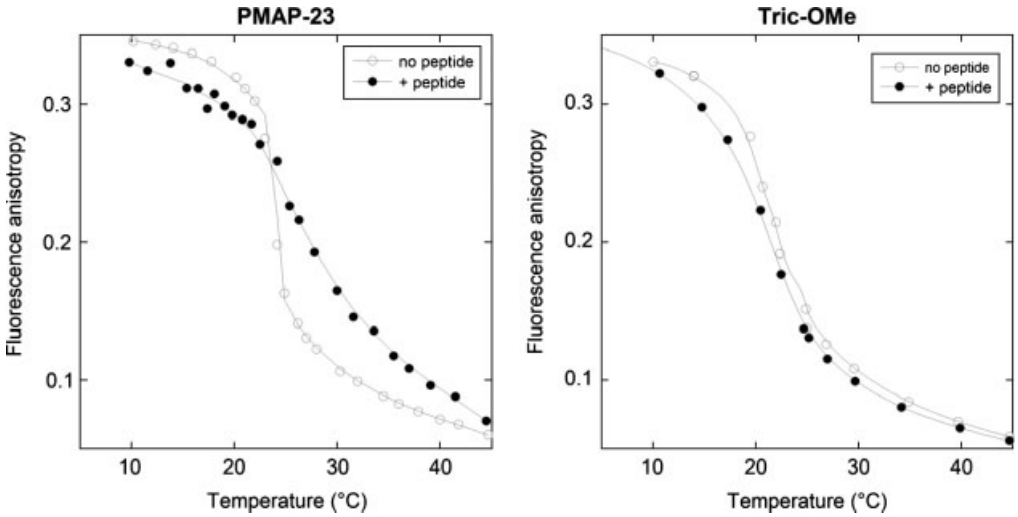

Figure 6. Effect of peptide–membrane interactions on the thermotropic phase transition of dimyristoyl phospholipid vesicles, as followed by measuring the fluorescence anisotropy of DPH. Left: DMPC/DMPG (2 : 1) vesicles in the absence (empty circless) and in the presence of PMAP-23 (full circles). Right: DMPC vesicles in the absence (empty symbols) and in the presence of the equipotent trichogin GA IV analogue Tric-OMe (full symbols).

depth, with its charged side chains interacting strongly with the phospholipid polar heads. In this position, it causes a severe membrane perturbation, basically for an excluded volume effect: indeed, a single PMAP-23 molecule occupies the surface area of approximately ten lipids, and therefore, when many peptide molecules bind to the outer layer of a cellular membrane, a tension rapidly builds up between the two leaflets of the bilayer, eventually leading to the formation of membrane defects. In addition, PMAP-23 insertion perturbs the order of the lipid chains in the bilayer. In essence, this is the ''Shai-Matsuzaki-Huang'' or ''carpet'' model of pore formation.

However, the neutral, distinctly hydrophobic, peptaibol trichogin GA IV, does not cause any significant membrane perturbation when it is bound parallel to the membrane surface, i.e. in its most stable orientation at low peptide/lipid ratios [28]. This is probably a consequence of its smaller size, but also of its deeper position inside the membrane (as compared to PMAP-23) and of its ability to ''dissolve'' in the medium formed by the lipid acyl chains. For this same reason, also a transmembrane peptide orientation is possible in the case of trichogin GA IV. This peptide arrangement is populated only transiently at low peptide/lipid ratios (allowing trichogin GA IV translocation between the two membrane leaflets), but becomes predominant with increasing membrane-bound peptide concentration [28]. Our previous studies have shown that in this inserted orientation trichogin molecules tend to aggregate, leading to the formation of pores [28]. However, the structure of these channels was not clear, because the trichogin GA IV helix is much shorter than the thickness of an unperturbed bilayer. The simulations presented here suggested that trichogin GA IV, when inserted in a transmembrane orientation, causes a significant thinning of the bilayer, and it might thus be able to be in contact with both membrane surfaces at the same time. Therefore, a normal ''barrel-stave'' arrangement, with the peptide chains aggregated laterally to form a cylinder superstructure, the inner water-filled lumen of which is lined by the hydrophilic sides of the helices, could be sufficient to describe the mechanism of pore formation even for such a relatively short peptide.

Acknowledgements

This project was supported by the Italian Ministry of Foreign Affairs, the Italian Ministry of University and Research (PRIN 2006) and by the Korea Foundation for International Cooperation of Science & Technology (KIKOS) (K20713000012-07B0100-01210). Computational resources were kindly made available by the Fermi and CASPUR Research Centers (Rome).

References

1 Hancock REW, Sahl HG. Antimicrobial and host-defense peptides as new anti-infective therapeutic strategies. *Nat. Biotech.* 2006; **24**: 1551–1557.
2 Shai Y. Mode of action of membrane active antimicrobial peptides. *Biopolymers* 2002; **66**: 236–248.
3 Zasloff M. Antimicrobial peptides of multicellular organisms. *Nature* 2002; **415**: 389–395.
4 Marr AK, Gooderham WJ, Hancock REW. Antibacterial peptides for therapeutic use: obstacles and realistic outlook. *Curr. Opin. Pharmacol.* 2006; **6**: 468–472.
5 Tossi A, Sandri L. Molecular diversity in gene-encoded, cationic antimicrobial polypeptides. *Curr. Pharm. Des.* 2002; **8**: 743–761.
6 Giangaspero A, Sandri L, Tossi A. Amphipathic α-helical antimicrobial peptides. *Eur. J. Biochem.* 2001; **268**: 5589–5600.
7 Mueller P. Membrane excitation through voltage-induced aggregation of channel precursors. *Ann. N. Y. Acad. Sci.* 1975; **264**: 247–264.
8 Stella L, Burattini M, Mazzuca C, Palleschi A, Venanzi M, Baldini C, Formaggio F, Toniolo C, Pispisa B. Alamethicin interaction with lipid membranes: a spectroscopic study on synthetic analogues. *Chem. Biodivers.* 2007; **4**: 1299–1312.
9 Qian S, Wang W, Yang L, Huang HW. Structure of the alamethicin pore reconstructed by X-ray diffraction analysis. *Biophys. J.* 2008; **94**: 3512–3522.
10 Tieleman DP, Hess B, Sansom MS. Analysis and evaluation of channel models: simulations of alamethicin. *Biophys. J.* 2002; **83**: 2393–2407.
11 Gazit E, Miller IR, Biggin PC, Sansom MS, Shai Y. Structure and orientation of the mammalian antibacterial peptide cecropin P1 within phospholipid membranes. *J. Mol. Biol.* 1996; **258**: 860–870.
12 Matsuzaki K, Murase O, Tokuda H, Funakoshi S, Fujii N, Miyajima K. Orientational and aggregational states of magainin 2 in phospholipid bilayers. *Biochemistry* 1994; **33**: 3342–3349.
13 Ludtke SJ, He K, Heller WT, Harroun, TA, Yang L, and Huang HW. Membrane pores induced by magainin. *Biochemistry* 1996; **35**: 13723–13728.

14 Leontiadou H, Mark AE, Marrink SJ. Antimicrobial peptides in action. *J. Am. Chem. Soc.* 2006; **128**: 12156–12161.
15 Sengupta D, Leontiadou H, Mark AE, Marrink SJ. Toroidal pores formed by antimicrobial peptides show significant disorder. *Biochim. Biophys. Acta* 2008; **1778**: 2308–2317.
16 Pokorny A, Birkbeck TH, Almeida PFF. Mechanism and kinetics of δ-lysin interaction with phospholipid vesicles. *Biochemistry* 2002; **41**: 11044–11056.
17 Zhao H, Sood R, Jutila A, Bose S, Fimland G, Nissen-Meyer J, Kinnunen PKJ. Interaction of the antimicrobial peptide pheromone Plantaricin A with model membranes: implications for a novel mechanism of action. *Biochim. Biophys. Acta* 2006; **1758**: 1461–1474.
18 Sevcsik E, Pabst G, Jilek A, Lohner K. How lipids influence the mode of action of membrane-active peptides. *Biochim. Biophys. Acta* 2007; **1768**: 2586–2595.
19 Ladokhin AS, White SH. 'Detergent-like' permeabilization of anionic lipid vesicles by melittin. *Biochim. Biophys. Acta* 2001; **1514**: 253–260.
20 Bechinger B, Lohner K. Detergent-like actions of linear amphipathic cationic antimicrobial peptides. *Biochim. Biophys. Acta* 2006; **1758**: 1529–1539.
21 Lacapère, JJ, Pebay-Peyroula E, Neumann JM, Etchebest C. Determining membrane protein structures: still a challenge! *Trends Biochem. Sci.* 2007; **32**: 259–270.
22 Orioni B, Bocchinfuso G, Kim JY, Palleschi A, Grande G, Bobone S, Venanzi M, Park Y, Kim JI, Hahm KS, Stella L. Membrane perturbation by the antimicrobial peptide PMAP-23: a fluorescence and molecular dynamics study. *Biochim. Biophys. Acta* (in press). DOI:10.1016/j.bbamem.2009.04.013.
23 Stella L, Venanzi M, Hahm KS, Formaggio F, Toniolo C, Pispisa B. Shining a light on peptide-membrane interactions. Fluorescence methods in the study of membrane-active peptides. *Chemistry Today* 2008; **26**: 44–46.
24 Matyus E, Kandt C, Tieleman DP. Computer simulation of antimicrobial peptides. *Curr. Med. Chem.* 2007; **14**: 2789–2798.
25 Khandelia H, Ipsen JH, Mouritsen OG. The impact of peptides on lipid membranes. *Biochim. Biophys. Acta* 2008; **1778**: 1528–1536.
26 Esteban-Martín S, Salgado J. Self-assembling of peptide/membrane complexes by atomistic molecular dynamics simulations. *Biophys. J.* 2007; **92**: 903–912.
27 Stella L, Mazzuca C, Venanzi M, Palleschi A, Didonè M, Formaggio F, Toniolo C, Pispisa B. Aggregation and water-membrane partition as major determinants of the activity of the antibiotic peptide trichogin GA IV. *Biophys. J.* 2004; **86**: 936–945.
28 Mazzuca C, Stella L, Venanzi M, Formaggio F, Toniolo C, Pispisa B. Mechanism of membrane activity of the antibiotic trichogin GA IV: a two-state transition controlled by peptide concentration. *Biophys. J.* 2005; **88**: 3411–3421.
29 Gatto E, Mazzuca C, Stella L, Venanzi M, Toniolo C, Pispisa B. Effect of peptide lipidation on membrane perturbing activity: a comparative study on two trichogin analogues. *J. Phys Chem. B* 2006; **110**: 22813–22818.
30 Pispisa B, Stella L, Mazzuca C, Venanzi M. Trichogin topology and activity in model membranes as determined by fluorescence spectroscopy. In *Reviews in Fluorescence 2006*, Geddes CD, Lakowicz JR (eds.). Springer: New York, 2006; 47–70.
31 Venanzi M., Gatto E, Bocchinfuso G, Palleschi A, Stella L, Formaggio F, Toniolo C. Dynamics of formation of a helix-turn-helix structure in a membrane-active peptide: a time-resolved spectroscopic study. *ChemBioChem* 2006; **7**: 43–45.
32 Venanzi M, Gatto E, Bocchinfuso G, Palleschi A, Stella L, Baldini C, Formaggio F, Toniolo C. Peptide folding dynamics: a time-resolved study from the nanosecond to the microsecond time regime. *J. Phys. Chem. B* 2006; **110**: 22834–22841.
33 Zanetti M, Storici P, Tossi A, Scocchi M, Gennaro R. Molecular cloning and chemical synthesis of a novel antimicrobial peptide derived from pig myeloid cells. *J. Biol. Chem.* 1994; **269**: 7855–7858.
34 Kang JH, Shin SY, Jang SY, Kim KL, Hahm KS. Effects of tryptophan residues of porcine myeloid antibacterial peptide PMAP-23 on antibiotic activity. *Biochem. Biophys. Res. Comm.* 1999; **264**: 281–286.
35 Lee DG, Kim DH, Park Y, Kim HK, Kim HN, Shin YK, Choi CH, Hahm KS. Fungicidal effect of an antimicrobial peptide, PMAP-23, isolated from porcine myeloid, against *Candida albicans*. *Biochem. Biophys. Res. Commun.* 2001; **282**: 570–574.
36 Park K, Oh D, Shin SY, Hahm KS, Kim Y. Structural studies of porcine myeloid antibacterial peptide PMAP-23 and its analogues in DPC micelles by NMR spectroscopy. *Biochem. Biophys. Res. Commun.* 2002; **290**: 204–212.
37 Yang ST, Jeon JH, Kim Y, Shin SY, Hahm KS, Kim JI. Possible role of a PXXP central hinge in the antibacterial activity and membrane interaction of PMAP-23, a member of the cathelicidin family. *Biochemistry* 2006; **45**: 1775–1784.
38 Brown KL, Hancock REW. Cationic host defense (antimicrobial) peptides. *Curr. Opin. Immunol.* 2006; **18**: 24–30.
39 Peggion C, Formaggio F, Crisma M, Epand RF, Epand RM, Toniolo C. Trichogin: a paradigm for lipopeptaibols. *J. Pept. Sci.* 2003; **9**: 679–689.
40 De Zotti M, Biondi B, Formaggio F, Toniolo C, Stella L, Park Y, Hahm KS. Trichogin GA IV: an antibacterial and protease-resistant peptide. *J. Pept. Sci.* this issue.
41 Toniolo C, Brückner H. Peptaibiotics. *Chem. Biodivers.* 2007; **4**: 1021–1022.
42 Duclohier H. Peptaibiotics and peptaibols. An alternative to classical antibiotics? *Chem. Biodivers.* 2007; **4**: 1023–1026.
43 Chugh JK, Wallace BA. Peptaibols: models for ion channels. *Biochem. Soc. Trans.* 2001; **29**: 565–570.
44 Leitgeb B, Szekeres A, Manczinger L, Vágvölgyi C, Kredics L. The history of alamethicin: a review of the most extensively studied peptaibol. *Chem. Biodivers.* 2007; **4**: 1027–1051.
45 Toniolo C, Crisma M, Formaggio F, Peggion C, Monaco V, Goulard C, Rebuffat S, Bodo B. Effect of N^{α}-acyl chain length on the membrane-modifying properties of synthetic analogs of the lipopeptaibol trichogin GA IV. *J. Am. Chem. Soc.* 1996; **118**: 4952–4958.
46 Toniolo C, Peggion C, Crisma M, Formaggio F, Shui X, Eggleston DS. Structure determination of racemic trichogin A IV using centrosymmetric crystals. *Nat. Struct. Biol.* 1994; **1**: 908–914.
47 Tieleman DP; Sansom MSP, Berendsen HJC. Alamethicin helices in a bilayer and in solution: molecular dynamics simulations. *Biophys. J.* 1999; **76**: 40–49.
48 van der Spoel D, Lindahl E, Hess B, Groenhof G, Mark AE, Berendsen HJC. GROMACS: fast, flexible, and free. *J. Comput. Chem.* 2005; **26**: 1701–1718.
49 Berendsen, H. J. C.; Postma, J. M.; van Gunsteren, W. F.; Hermans, J. In: *Intermolecular forces*, Pullman B. (ed.). Reidel Publishing Company: Dordrecht. 1981; pp 331–342.
50 Miyamoto S, Kollman PA. SETTLE: an analytical version of the SHAKE and RATTLE algorithms for rigid water models. *J. Comput. Chem.* 1992; **13**: 952–962.
51 Berger O, Edholm O, Jähnig F. Molecular dynamics simulations of a fluid bilayer of dipalmitoylphosphatidylcholine at full hydration, constant pressure, and constant temperature. *Biophys. J.* 1997; **72**: 2002–2013.
52 Marrink SJ, Berger O, Tieleman DP, Jaehnig F. Adhesion forces of lipids in a phospholipid membrane studied by molecular dynamics simulations. *Biophys. J.* 1998; **74**: 931–943.
53 Berendsen HJC, Postma JPM, van Gunsteren WF, Di Nola A, Haak JR. Molecular dynamics with coupling to an external bath. *J. Chem. Phys.* 1984; **81**: 3684–3690.
54 Hess B, Bekker H, Berendsen HJC, Fraaije JGEM. LINCS: a linear constraint solver for molecular simulations. *J. Comput. Chem.* 1997; **18**: 1463–1472.
55 Darden T, York D, Pedersen L. Particle mesh Ewald: an $N \cdot \log(N)$ method for Ewald sums in large systems. *J. Chem. Phys.* 1993; **98**: 10089–10092.
56 Essmann U, Perera L, Berkowitz ML, Darden T, Lee H, Pedersen LG. A smooth particle mesh Ewald method. *J. Chem. Phys.* 1995; **103**: 8577–8592.
57 Feenstra KA, Hess B, Berendsen HJC. Improving efficiency of large time-scale molecular dynamics simulations of hydrogen-rich systems. *J. Comput. Chem.* 1999; **20**: 786–798.
58 Humphrey W, Dalke A, Shulten K. VMD: visual molecular dynamics. *J. Mol. Graph.* 1996; **14**: 33–38.
59 Egberts E, Marrink SJ, Berendsen HJC. Molecular dynamics simulation of a phospholipid membrane. *Eur. Biophys. J.* 1994; **22**: 423–4.
60 Marrink SJ, Lindhal E, Edholm O, Mark AE. Simulation of the spontaneous aggregation of phospholipids into bilayers. *J. Am. Chem. Soc.* 2001; **123**: 8638–8639.

61 de Vries AH, Mark AE, Marrink SJ. Molecular dynamics simulation of the spontaneous formation of a small dppc vesicle in water in atomistic detail. *J. Am. Chem. Soc.* 2004; **126**: 4488–4489.
62 Leontiadou H, Mark AE, Marrink SJ. Molecular dynamics simulations of hydrophilic pores in lipid bilayers. *Biophys. J.* 2004; **86**: 2156–2164.
63 Salnikov ES, Erilov DA, Milov AD, Tsvetkov YD, Peggion C, Formaggio F, Toniolo C, Raap J, Dzuba SA. Location and aggregation of the spin-labeled peptide trichogin GA IV in a phospholipid membrane as revealed by pulsed EPR. *Biophys. J.* 2006; **91**: 1532–1540.
64 Jähnig F. Structural order of lipids and proteins in membranes: evaluation of fluorescence anisotropy data. *Proc. Natl. Acad. Sci. USA* 1979; **76**: 6361–6365.
65 de Planque MRR, Greathouse DV, Koeppe II RE, Schäfer H, Marsh D, Killian JA. Influence of lipid/peptide hydrophobic mismatch on the thickness of diacylphosphatidylcholine bilayers. A ^{2}H NMR and ESR study using designed transmembrane α-helical peptides and gramicidin A. *Biochemistry* 1998; **37**: 9333–9345.
66 Duque D, Li XJ, Katsov K and Schick M. Molecular theory of hydrophobic mismatch between lipids and peptides. *J. Chem. Phys.* 2002; **116**: 10478.
67 Kandasamy SK, Larson RG. Molecular dynamics simulations of model trans-membrane peptides in lipid bilayers: a systematic investigation of hydrophobic mismatch. *Biophys. J.* 2006; **90**: 2326–2343.

